Technical Report 2012-003:

Arterial Input Function without Blood Sampling: a Probabilistic Approach. Proof of Concept and Application to Cardiac PET-FDG in rodents

R. Mabrouk[1,2], S. Prevost[2], F. Dubeau[3], and L. Bentabet[4]

[1]Departments of Computer Sciences, [2]Departments of Nuclear Medicine and,
[3]Departments of Mathematics Université de Sherbrooke (Qc)

[4]Department of Computer Science, Bishop's University

Abstract

Serial arterial blood sampling in dynamic positron emission tomography (PET) studies can be eliminated by using a left ventricular time-activity curve as an input function (IF) obtained from user drawn regions of interest (ROIs) followed by application of appropriate correction factors. In this paper, we propose a new approach based on the decomposition of image pixel intensity into blood and tissue components using Bayesian statistics. The method uses an *a priori* knowledge of the probable distribution of blood and tissue in the images. Likelihood measures are derived from regions of interest (ROI) manually drawn around the blood and tissue pools. Bayes' rule is then applied to compute weights that account for the concentrations of the radiotracer in blood and tissue and their relative contribution in each image pixel. We tested the method on 18 dynamic cardiac FDG-PET of normal rats.

Our approach generates tissue glucose metabolic values comparable to those obtained with manual blood sampling ($p<0.05$). The reference MMRG calculated with sampled IF differs by only 3% from the value calculated with our method. The benefit of employing the proposed approach is its simplicity, computationally efficiently, and its high reproducibly. It directly separates the blood components from tissue regions, without requiring further operations such as non-negativity constraints, as opposed to other methods.

Keywords: PET, Kinetic Modeling, Input Function, Bayes Rule.

I. INTRODUCTION

Imaging the bio-distribution and kinetics of radiopharmaceuticals with positron emission tomography (PET) is a valuable tool to assess a variety of physiological parameters. These parameters depend on biochemical transformations, which can be represented by compartments. The widely used method to extract physiological parameters using PET images is compartmental modeling. This method uses measured images but requires an input function (IF) to account for the delivered radiotracer to the tissue. [^{18}F]-Fluoro-Deoxy-Glucose (^{18}F-FDG) is a tracer, which is widely used as a glucose analog. Glucose kinetic modeling can be used to quantitatively measure the rate of glucose metabolism and to explore the pathophysiology of diseases such as heart failure [1], among others.

Up to now, the invasive gold standard arterial plasma sampling procedure to obtain IF remains the reference. This method for obtaining IF has been intensively investigated [2–5].

Unfortunately, this method has many inconveniences. The large number of blood samples required can alter the circulation dynamics in small animals due to blood loss. Manipulation of the samples provides unnecessary radiation dose to researchers. The blood samples need to be measured in well counters for radiotracer concentration cross-calibrated with the PET scanner, and interpolated at the image scanning times during kinetic modeling. All these operations are either invasive, cumbersome, or add uncertainties to the calculated final values. An alternative to manual blood sampling is the automatic blood sampling technique [6–9]. The automatic withdrawing of blood samples minimizes the risk of radiation exposure for the operator, but additional corrections are required to accurately determine IF. Additionally, this method has many drawbacks such as the time delay and dispersion in the tubing, the contamination of the samples in the tubing, and the cross-calibration between sample detection setup and the PET scanner [10].

To avoid the difficulties encountered in withdrawing and measuring the blood samples in each experience, and when performing studies in similar protocols, population-based IFs have been proposed, which might be sufficient for many applications. For these functions to be properly used in kinetic modeling, only one or a few blood samples are extracted from the subject to normalize the averaged IF [11–13]. For the same objective, other authors have relied on extraction of the IF from images [14–17]. To increase the accuracy of the method, the data can be corrected for the spillover from blood to tissue and from tissue to blood.

Other alternative methods of estimating IF from images have been proposed. Buvat *et al.* [18] have used the factor analysis of dynamic structures (FADS) method which decomposes the dynamic sequences into component images. IF is then extracted from the blood component's images [19-21]. The independent component analysis (ICA) is

another method which has been applied to extract IF from PET images [22-27]. ICA acts in similar fashion as FADS but uses a de-mixing matrix to isolate components from a mixture. In some studies [28, 29], authors have presented a method of IF extraction from the so-called image-derived input function (IDIF). IF can also be obtained by the simultaneous estimation method, based on a multi-exponential time-activity function scaled to the measured activity concentration in a limited number of blood samples [30].

In this paper, we introduce a new approach based on the decomposition of image pixel's intensity into blood and tissue components. The method uses Bayes rule to combine the prior knowledge of the probable distribution of blood and tissue in the images calculated in the time axis with likelihood probabilities estimated from the space domain. The proposed approach allows calculating images of blood and tissue components and their time-activity curves. Additionally, our calculations are based on statistics already used in most of the aforementioned references, i.e. exponential distribution for blood and bi-exponential model for tissue.

II. MATERIALS AND METHODS

II-1 PET Measurements

The animal experiments were conducted in accordance with the recommendations of the Canadian Council on Animal Care and of the Committee of Ethics for Animal Experiments at the Faculty of Medicine and Health Sciences, Sherbrooke University. Experiments were performed on eighteen male Fischer rats of 200g ± 22g. The animals had free access to food and water throughout the study. Forty minutes dynamic acquisitions in list-mode were performed on the Sherbrook's small animal PET scanner (LabPET4). A venous catheter was installed into the caudal vein for the radiotracer injection. The injection of 50 ± 5 MBq of FDG in a volume of 400 µL was done over the course of 1 minute using an automatic infusion pump in the tail vein. The rats were prepared and imaged while under anesthesia with isoflurane (1.5 % volume and 1 L/min oxygen flow, Abbott Laboratories) delivered through a nose cone. A PE50 polyethylene catheter (Becton Dickinson) was inserted into the femoral artery for blood sampling. The preparation of the animals took around 20 minutes. During imaging, heart and respiration rates were monitored with an ECG and a respiration pillow (model 1025L SAII). A dynamic series of 27 frames were sorted out from the list-mode data, using the following sequence: 12 × 10 sec, 6 × 30 sec, 6 × 150 sec, 2 x 5 min, and a final frame of 10 min. Image slices were reconstructed on a 160 × 160 matrix with a 0.5 × 0.5 pixel size using the Maximum Likelihood Expectation Maximization (ML-EM) algorithm [31]. The signal-to-noise ratio (SNR) was analyzed with conventional method which are based on the signal standard deviation in a ROI in the background and the signal mean in a ROI in the image for several regions of interest (ROIs) which were reconstructed with 10, 15 and

20 iterations and it has given respectively 49.03 dB, 47.88 dB and 47.19 dB. 10 iterations were kept for the study.

During the acquisition, blood was withdrawn through the femoral catheter at 20, 40, 50, 60, 70, 90, 120, 150, 180 sec and at 5, 10, 15, 20, 25, 35 min. The blood time-activity curves were generated from a linear interpolation of the blood sampling data to the PET dynamic series of 27 frames. Thirty minutes after the injection, the glucose level was obtained from the plasma analysis using a commercial reagent kit (Siemens Healthcare Diagnostic Inc., Deerfield, IL, USA) and an automated clinical chemistry analyzer (Dimension Xpand Plus, Siemens Healthcare Diagnostic Inc., IL, USA).

II-2 Kinetic Modeling

Figure 1 depicts the three-compartment FDG model used in our study for estimating the rate constants ($K_1 - k_4$), and the myocardium metabolic rate of glucose (MMRG) where $C_f(t)$ represents the concentration of the free FDG in tissue, $C_m(t)$ is the concentration of the phosphorylated FDG (FDG-6-PO4) in tissue and $C_p(t)$ is the plasma time activity curve. It refers to the IF for the model. The sum of C_f and C_m (which is the tissue time-activity curve ($tTAC$)) plus a blood volume vascular fraction $\vartheta(0 \leq \vartheta < 1)$ of C_p produces the measured data C_{PET}. The differential equations describing the FDG kinetic behavior are given by [32]:

$$\frac{dC_f(t)}{dt} = K_1 C_f(t) - (k_2 + k_3)C_f(t) + k_4 C_m(t),$$

$$\frac{dC_m(t)}{dt} = k_3 C_f(t) - k_4 C_m(t), \quad (1)$$

$$C_{PET}(t) = \left(C_f(t) + C_m(t)\right) + \vartheta C_p(t),$$

where K_1 refers to the rate of delivery of the tracer to tissue in units of volume of blood per mass of tissue per minute (mL/g/min) and k_2, k_3, k_4 are the transport rate constants in units of min^{-1}. $C_{PET}(t)$ is given by:

$$C_{PET}(t) = \left(\frac{K_1}{\alpha_2 + \alpha_1}[(k_3 + k_4 - \alpha_1)e^{-\alpha_1 t} + (\alpha_2 - k_3 - k_4)e^{-\alpha_2 t}] \otimes C_p(t)\right) + \vartheta C_p(t), \quad (2)$$

where:

$$\alpha_1 = \left[k_2 + k_3 + k_4 - \sqrt{(k_2 + k_3 + k_4)^2 - 4k_2k_4}\right]/2$$

$$\alpha_2 = \left[k_2 + k_3 + k_4 + \sqrt{(k_2 + k_3 + k_4)^2 - 4k_2k_4}\right]/2$$

The symbol $\otimes$ in (2) indicates the convolution operation. The MMRG is defined by:

$$MMRG(\mu mole/100g/\text{min}) = 100\frac{gl}{LC}K$$

where gl is the glycemia value in $mmol/L$, $K = \frac{K_1\, k_3}{k_2+k_3}$ the influx rate constant and LC = 1 is the lumped constant accounting for the utilization of FDG versus glucose which is the natural substrate.

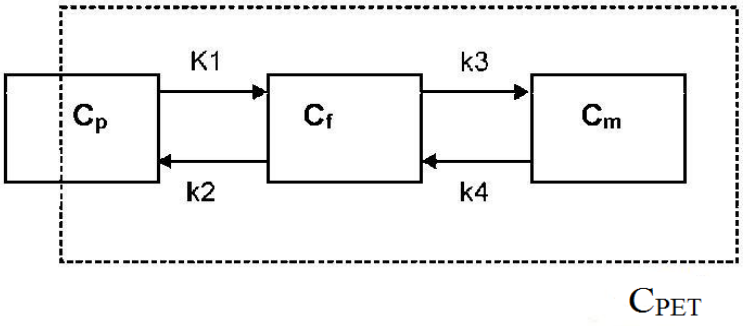

Figure 1- Three-compartment model: A two-tissue plus plasma compartmental model representing ^{18}F-FDG kinetics in tissue. Dashed line represents PET measure. Compartment C_f represents tracer in extra-vascular extra-cellular space. Compartment C_m represents the phosphorylated ^{18}F-FDG in tissue. *K1-k4* are the rate constants to be calculated.

Knowing $C_{PET}(t)$ and $C_p(t)$ on several time point, it is possible to determine the parameters $K_1$to k_4 by nonlinear least squares fitting. In next section, we present how we calculate an accurate $C_p(t)$ and a $tTAC(t)$ from image data.

II-3 Bayesian Approach

The Bayesian approach is widely used in the literature for data classification [33, 34]. In this article, it is used to estimate the blood time course activity $C_p(t)$ and the tissue uptake $tTAC(t)$ from a PET image sequence data. We consider the PET data as a collection of τ spatially registered images. Only a region of interest (ROI) S of size N manually drawn around the heart is considered in the sequel. The activity within S is modeled by a random field X^t , where $t = 1, \cdots, \tau$ refers to the time index of the image within the PET sequence. The value of X^t at a point $s \in S$ will be written as x_s^t. We

consider the PET measurement as a mixture of two distinct components, which are the blood activity and the tissue activity. Consequently, X^t is modeled as a mixture of two random processes, X_B^t which models the blood component and X_T^t which models the tissue component. The values of X_B^t and X_T^t at a pixel $s \in S$ will be written as $x_{B,s}^t$ and $x_{T,s}^t$. Similarly, S is spatially split into two parts, S_B and S_T, where S_B is a ROI manually drawn around the left ventricular chamber and S_T is a ROI manually drawn around the myocardium (see Figure 3).

We model the blood activity $x_{B,s}^t$ as a fraction of x_s^t. Thus:

$$x_{B,s}^t = \begin{cases} \alpha_{B,s}^t \, x_s^t \,, & s \in S_B \\ \left(1 - \alpha_{T,s}^t\right) x_s^t, & s \in S_T \end{cases} \tag{3}$$

Similarly, the tissue activity is given by:

$$x_{T,s}^t = \begin{cases} \left(1 - \alpha_{B,s}^t\right) x_s^t, & s \in S_B \\ \alpha_{T,s}^t \, x_s^t \,, & s \in S_T \end{cases} \tag{4}$$

In (3) and (4), $\alpha_{B,s}^t \in [0,1]$ and $\alpha_{T,s}^t \in [0,1]$ are the actual fractions of blood and tissue activities at each pixel $s \in S$ at time $t = 1, \cdots, \tau$. In the following, we estimate these fractions from the measured X^t using a Bayesian framework. We assume that the intensities of each component of X^t (*i.e.* X_B^t *and* X_T^t) follow conditional probability functions (p.d.f) $p(x_s^t|X_B^t)$ and $p(x_s^t|X_T^t)$. P.d.f. $p(x_s^t|X_B^t)$ (respectively $p(x_s^t|X_T^t)$) expresses the likelihood of observing x_s^t given a blood activity (respectively a tissue activity). The probability of observing a blood activity (respectively a tissue activity) is a prior knowledge that we model through prior probability $p(X_B^t)$ (respectively $p(X_T^t)$).

Given this framework, we define the blood fraction $\alpha_{B,s}^t$ as being the probability of observing a blood activity X_B^t given observation x_s^t, or

$\alpha_{B,s}^t \stackrel{\text{def}}{=} p(X_B^t|x_s^t)$.

Using the Bayes' rule one obtains

$$\alpha_{B,s}^t = \frac{p(x_s^t|X_B^t)p(X_B^t)}{\sum_{i=B,T} p(x_s^t|X_i^t)\, p(X_i^t)} \tag{5}$$

Similarly, the tissue fraction is defined as:

$\alpha_{T,s}^t \stackrel{\text{def}}{=} p(X_T^t|x_s^t)$,

then

$$\alpha_{T,s}^{t} = \frac{p(x_s^t|X_T^t)\, p(X_T^t)}{\sum_{i=B,T} p(x_s^t|X_i^t)\, p(X_i^t)} \tag{6}$$

In Bayesian framework, evaluating the likelihood in (5) and (6) is often hard and much of the research in this area has focused on ways of doing it [35]. A simple, but reasonably good approximation of $p(x_s^t|X_B^t)$ and $p(x_s^t|X_T^t)$ is given by:

$$p(x_s^t|X_B^t) = \frac{n_B(x_s^t)}{N_B} \tag{7}$$

$$p(x_s^t|X_T^t) = \frac{n_T\,(x_s^t)}{N_T} \tag{8}$$

where $n_B(x_s^t)$ and $n_T(x_s^t)$ are respectively the number of pixels in S_B and S_T having intensity x_s^t. N_B and $N_T$refer to the size of S_B and S_T. Figure 2 (A-B) shows the likelihoods calculated from the last image of the sequence.

To compute $p(X_B^t)$, we propose to use the prior knowledge of the time acquisition's frequency. The dynamic PET data frames are acquired in time according to a predefined schedule. This schedule is represented by a time vector:

$$\Big(\underbrace{10sec, 20sec, \cdots, 120sec}_{12frames}, \underbrace{150sec, 180sec, \cdots, 300sec}_{6frames},$$

$$\underbrace{450sec, 600sec, \cdots, 1200sec}_{6frames}, \underbrace{1500sec, 1800sec}_{2frames}, \underbrace{2400sec}_{1frame}\Big)$$

The duration of each frame depends on the time of data recording. Duration is very short at early acquisition period to locate the activity peak of blood, and it is long at late acquisition period to see how the tracer diffuses into the tissue. The time vector is then sampled with a step of two minutes to calculate the frames' frequency at each time step. The resulting histogram $\{h(u)\}_{u=1}^{n}$is given in Figure 2(C), where u a time step index and n is is the time vector size. This histogram represents the prior knowledge of the tracer's temporal behavior, $p(X_B^t)$, in the PET data. Given its exponential-like shape, an exponential p.d.f. is used to fit the histogram data as follows:

$$p(X_B^t) = \begin{cases} \lambda \mathrm{e}^{-\lambda.\mathrm{t}} & \text{if } \mathrm{t} > 0 \\ 0 & \text{if } \mathrm{t} < 0 \end{cases} \tag{9}$$

where λ is a positive parameter that is estimated with maximum likelihood estimator as follows:

$$\lambda = \frac{n}{\sum_{u=1}^{n} h(u)}$$

Figure 2(C) depicts the prior distribution $p(X_B^t)$.

The tissue prior $p(X_T^t)$, depicted in Figure 2 (D), is computed from the FDG model as the response of tissue after a bolus injection. It follows from (2):

$$p(X_T^t) = \frac{K_1}{\alpha_1 + \alpha_2}[(k_3 + k_4 - \alpha_1)e^{-\alpha_1 t} + (\alpha_2 - k_3 - k_4)e^{-2t}] \otimes p(X_B^t), \qquad (10)$$

where K_1= 0.102 μmole/100g/min, k_2 = 0.13 min^{-1}, k_3 = 0.062 min^{-1}, and k_4= 0.0068 min^{-1}. These parameter values are representative of those usually obtained from studies in normal subjects [36].

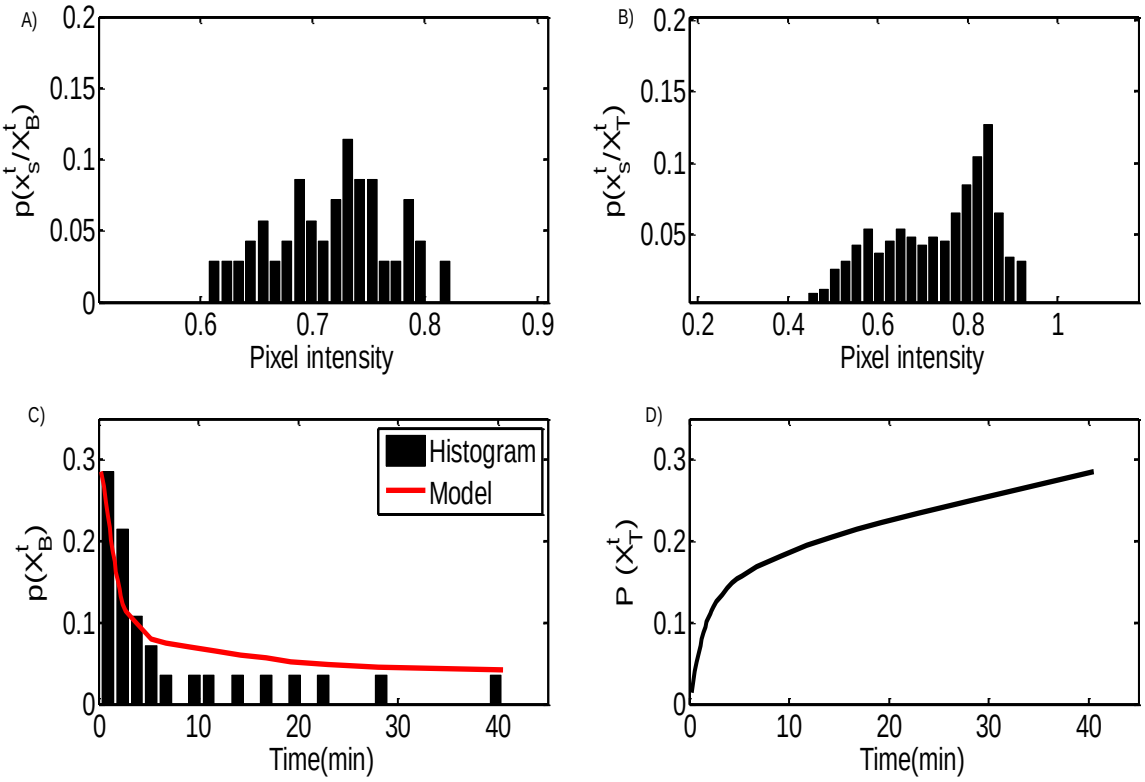

Figure 2 - (A) Likelihoods and priors calculated from S_B and S_T. (A) $p(x_s^t|X_B^t)$ calculated from the last frame blood pool region. (B) $p(x_s^t|X_T^t)$ calculated from the last frame tissue region. Intensities are

normalized between 0 and 1.(C) Prior probability of $p(X_B^t)$ after a bolus injection, the tracer diffuses into the tissue and consequently it exponentially decreases with time. The sampling of the temporal reconstructed images frequency allows the best way to assess the left ventricular blood diffusion to the tissue.(D)Prior probability of $p(X_T^t)$. The PET measurement in a tissue is viewed as the cumulative uptake response of the radiotracer diffused by blood. According to (.2), the consumption of the FDG molecule by the tissue is modeled by a bi-exponential convoluted by the IF which can be analytically reproduced to be used as a prior.

Our approach is summarized in Figure 3, which depicts how the initial PET image is processed to find the blood fraction and the tissue fraction images.

Once the component images are calculated, the time activity curve of each component is computed as the intensity average.

For the blood component, the time activity curve corresponds to the whole blood and it is calculated as follows:

$$C_w(t) = \frac{1}{N}\sum_{s\in S} x_{B,s}^t \tag{11}$$

$C_p(t)$ is computed from $C_w(t)$ using a correction factor $R_{BP}(t)$ as follows:

$$C_p(t) = R_{BP}(t)C_w(t), \tag{12}$$

where R_{BP} is calculated by taking a series of whole-blood samples throughout the course of several studies, centrifuging each sample into plasma and cellular components, and measuring the FDG concentration in each fraction. The resulting R_{BP} is time dependent as it is given by [37, 38].

$$R_{BP}(t) = 0.386\exp(-0.191\ t) + 1.165 \tag{13}$$

For the tissue component, the time activity curve is calculated as follows:

$$tTAC(t) = \frac{1}{N}\sum_{s\in S} x_{T,s}^t \tag{14}$$

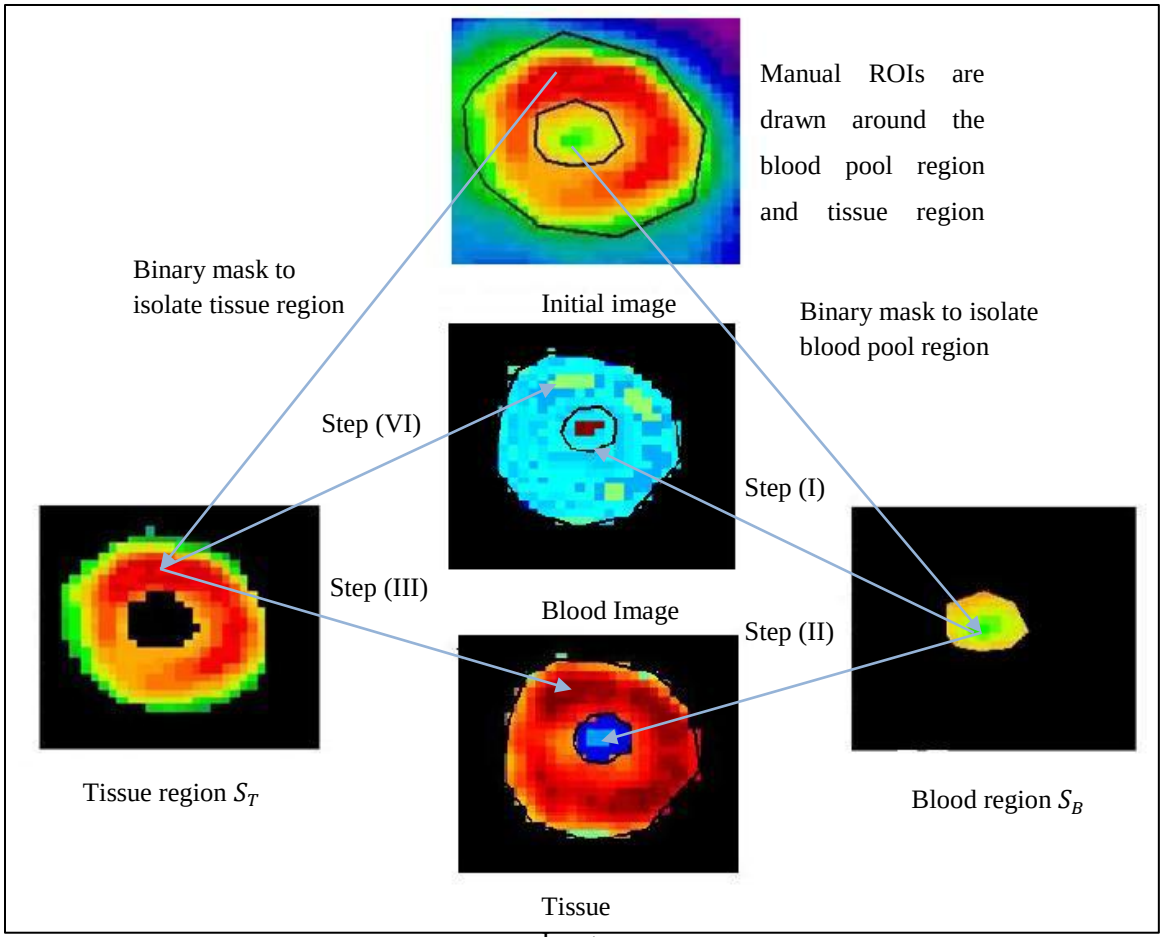

Figure 3 - Procedure for calculating the blood images and tissue images. Step (I) is the calculation of the blood fraction from the intensity of a pixel belonging to the blood pool region as $x_{B,s}^t = \alpha_{B,s}^t \cdot x_s^t$. The remaining intensity will be allocated to the same location for the tissue image in step (II) as $x_{T,s}^t = (1 - \alpha_{T,s}^t) \cdot x_s^t$. Similarly, for a pixel belonging to the tissue region, we calculate in step (IV) the fraction of blood as $x_{B,s}^t = (1 - \alpha_{B,s}^t) \cdot x_s^t$ and the fraction of tissue for the same pixel as $x_{T,s}^t = \alpha_{T,s}^t x_s^t$ in step (III)

III. RESULTS

Our approach allows to isolate the fractions of blood and tissue in each pixel of the PET image. Consequently, it allows the generation of blood and tissue image sequences with low cross-contamination. Figure 4 (A) shows the last frame of the initial PET image and illustrates appropriately the contamination effect, which makes it difficult to extract a true activity from the initial data sequence when using an IDIF. The cross-contamination is due to the organ's movement and the limited spatial resolution of the PET scanner. Figure 4 (B) shows the tissue image obtained using (4). In this image, the myocardium has a homogeneous intensity, which corresponds to 40 minutes of tracer's delivery by the

blood. The blood activity calculated using (3) is shown in Figure 4 (C). As expected, this image shows a low intensity of the radiotracer activity in the blood pool region in comparison with the image in Figure 4(A).

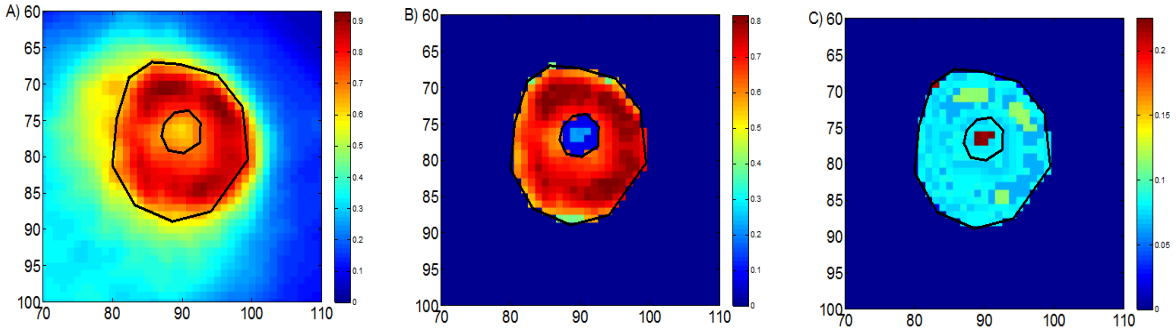

Figure 4 - Image of the rat heart measured with FDG during 40 min. (A) last frame of the PET image sequence. (B) last frame of the tissue image sequence computed by (4). (C) last image of the blood image sequence computed by (3)

The extracted tissue and blood sequences were then used to compute the time activity curves. The obtained results are given in Figure 5 (A) shows the whole blood time activity $c_w(t)$, calculated using (11), the plasma time activity curve $c_p(t)$ after correction using (12) and the tissue time activity curve $tAC(t)$ calculated using (14). The prior $p(X_T^t)$ in (10) used for calculating $\alpha_{T,s}^t$was adjusted with realistic constants result from the three compartment model. Table 1 describes value of constants $K_1 - k_4$ presented as a mean and standard deviation (SD) of 5 simulation

Table.1: The value of constants K_1 *to* k_4 presented as a mean and standard deviation (SD) of 5 simulations. Values of constants $k_i$are stable.

Parameters	Initialization	Estimated Mean	SD
$K_1(mL/g/min)$	0.102	0.101	0.015
$k_2(min^{-1})$	0.131	0.130	0.047
$k_3(min^{-1})$	0.062	0.061	0.001
$k_4(min^{-1})$	0.006	0.006	0.002

Figure 5 (B) compares the computed $C_p(t)$ with the IDIF computed from a manually drawn ROI around the left ventricular chamber and the sampled plasma activity. The IDIF curve is higher than the computed curve and the sampled curves because of the cross-contamination. The Figure 5 (B) shows that the IF curve computed using our probabilistic approach is much closer to the one calculated from the sampled plasma.

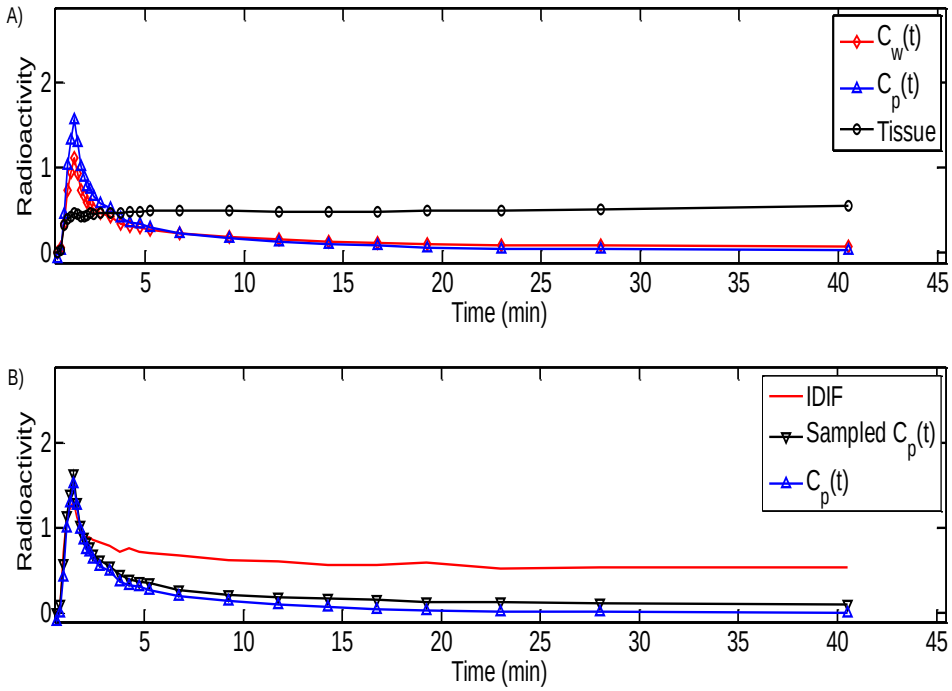

Figure 5 - Time activity curves from the same rat. (A), $tTAC(t)$, $C_w(t)$ and $C_P(t)$ time activity curves extracted from tissue and blood image components. (B) Comparison between sampled IF, IDIF and computed $C_p(t)$. The comparison illustrated in (B) shows clearly the close shape of the computed $C_p(t)$ to the sampling IF. In contrast spillover appear in the IDIF curve specially at the end of measure.

The MMRG values for the eighteen rats are computed separately using $C_p(t)$, the sampled IF and the IDIF. The results are reported as boxplots in Figure 6.

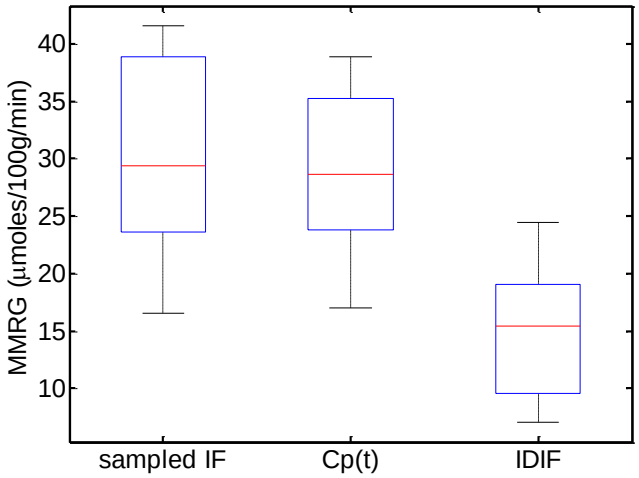

Figure.6 - Comparison of FDG MMRG values obtained with the sampled IF, the IDIF and the computed $C_p(t)$ for the eighteen rats. The t-test between MMRG of the sampled IF and $C_p(t)$ shows no significant difference (p<5%). The t-test between MMRG of the sampled IF and the IDIF shows a significant difference (p> 5%).

The t-test between MMRG calculated with sampled IF and calculated with $C_p(t)$ shows no significant difference (p<0.05). On the other hand, the t-test between MMRG calculated with the sampled IF and calculated with the IDIF shows a significant difference (p> 0.05). We can interpret quantitatively the difference existing in the MMRG values by computing relative errors between calculated MMRG. Indeed, the value calculated with our method differs by 3% from the gold standard whereas the value calculated with IDIF differs by 64%.

In order to study the robustness of the method with respect to the ROI, two processes have been applied and tested. First one, 100 random contours were generated from a manually traced contour around the blood pool on an area of 2 mm from the manually contour. The experiment showed a minimal change in MMRG value (standard deviation =1,15 $\mu mole/100g/$min). The second test consisted of two experts drawing the eighteen subjects ROIs, (the principal author and a nuclear medicine physician). The result showed that the variation of the area under curve (AUC) is minimal as illustrates in the Table 2 below.

Table.2: Relative error between AUC computed by user 1 and AUC computed by user 2 calculated as $\left|\frac{AUC1-AUC2}{AUC1}\right| \times 100$.The coefficient of correlation between the AUCs values is 99.6%, which shows a high reproducibility of ROI choices.

Rat index	1	2	3	4	5	6	7	8	9
Error of AUC(%)	3.0	2.8	3.5	7.6	0.4	1.5	3.2	3.1	1.8
Rat index	10	11	12	13	14	15	16	17	18
Error of AUC(%)	3.6	2.3	0.4	0.2	0.3	3.8	1.3	2.7	1.0

IV. DISCUSSION

The ability to define accurately IF is crucial for PET imaging research. In this regard, compartment modeling has long been the best way to analyze PET images. However, the blood-sampling procedure is still the reference in research. In small animals, this method has been a major barrier because of its invasive nature, the small size of blood vessels, and the animals' limited blood volume. Alternative solutions to obtain $C_p(t)$ from images include the IDIFs, the FADS and the ICA. Among these methods some do not require any blood sampling and others need just one sample to calibrate the IF. ICA was mostly used in human brain PET imaging and cardiac PET imaging. However, ICA has some pitfalls. The first one is that some components are sometimes projected entirely in the negative space, which requires a multiplication by (-1) as in the EPICA algorithm [23]. The second one is that the order of the identified independent components cannot be determined by the algorithm itself, requiring the intervention of an expert observer. Furthermore, as mentioned by Naganawa in [22], the signal of the estimated IF sometimes contains negative values in a portion of the curve, which requires more complex corrections or the use of alternative methods.

The FADS algorithm is another method which has been widely used to extract time activity curves from PET and SPECT images. However, it also suffers from data negativity problems, and statistical tools such as oblique analysis have to be used to project negative data into positive space. In contrast, IDIFs offer a very simple way to define $C_p(t)$ and tissue uptake. The disadvantage of this method is that the spillover effects make the IDIF a highly biased estimate as shown in Figure 5 (B). All these methods require the use of a recovery coefficient to compensate for the lack of resolution of the PET scanner versus the size of the vascular structure chosen for the input function

substitute. The probabilistic approach described in this paper offers a practical and robust method to correct the cross-contamination by estimating the fractions of free blood and free tissue activities from the initial PET image data sequence. The results reported in Figure 5 (B) show that the computed $C_p(t)$ is a valid and reliable estimate of the IF, and thus it can be used to derive accurately $k_1 - k_4$ and MMRG values. It does not rely on recovery coefficients. To illustrate how our method could be useful in the context of a medical diagnosis, we built parametric images which describe the MMRG value for each tissue pixel. The results are given in Figure 7.

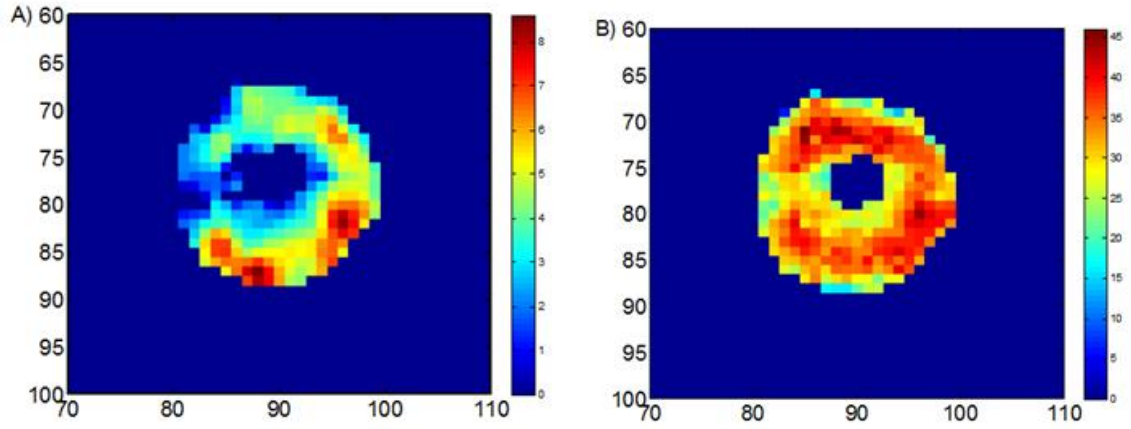

Figure 7 - Parametric MMRG image. Images are resized directly in units of glucose metabolism (micromole/100g/min). (A) Parametric MMRG image computed with sampled IF and x_s^t. (B) Parametric MMRG image computed with sampled IF and estimated $x_{s,T}^t$.

MMRG parametric images reflect the rate of glucose metabolism directly, rather than the radiotracer's concentration. The MMRG parametric image in Figure 7 (A) is computed using the sampled IF and x_s^t at each pixels $\in S_T$. This image corresponds to the MMRG before the correction for spillovers. The MMRG parametric image in Fig.7 (B) is computed using the sampled IF and $x_{s,T}^t$ at each pixel $s \in S_T$. This image corresponds to the MMRG after the correction for cross-contamination. In the case where no correction is applied on the image sequence, the estimated MMRG appears very low as indicated in Figure 7 (A). This is due to inadequate estimates of constants $K_1 - k_4$ from initial PET data shown in Fig.5 (A). By reducing the cross-contamination using our approach, we obtain MMRG values suitable for medical diagnosis as shown in Fig.7 (B).

The probabilistic approach described in this paper is easy to implement as standalone software or integrated into an existing one. In this work, we used the ventricular cavity activity as an IF but the algorithm could be used as well for the femoral and carotid arteries. It remains to be evaluated further in pathologic conditions as well as adapted for

other radiotracers. This is particularly important since $K_1 - k_4$ were obtained from a subgroup of normal subjects.

V. CONCLUSION

We demonstrated that the probabilistic estimation of the IF defined in this work is closely correlated to the true arterial blood curve for kinetic modeling of FDG studies without the difficulties of arterial blood sampling or complicated numerical analysis. For cardiac studies, this method requires only drawing ROIs around the interior blood-pool region of the left ventricle on the image as well as the ventricular region and the application of Bayes rule on calculated likelihoods and estimated priors. It is highly reproducible in PET-FDG of normal rat hearts but it remains to be validated in other circumstances.

VI. REFERENCES

[1] Abraham A, Nichol GK, Williams A *et al*. FDG PET Imaging of Myocardial Viability in an Experienced Center with Access to FDG and Integration with Clinical Management Teams: The Ottawa-FIVE Substudy of the PARR 2 Trial. J Nucl Med 2010; 51:567–74.

[2] Bedford RF, and Wollman H. Complications of percutaneous radial-artery cannulation: an objective prospective study in man. Anesthesiology 1973; 38:28–36.

[3] Jons PH, Ernst M, Hankerson J, Hardy K, and Zametkin AJ. Follow-up of radial arterial catheterization for positron emission tomography studies. Hum Brain Mapp 1997; 5:19–23.

[4] Bentourkia M, Bol A, Ivanoiu A, *et al*. A standardized blood sampling scheme in quantitative FDG-PET studies. IEEE Trans Med Imag 1999; 18:379-84.

[5] Erikson L and Kanno I. Blood sampling devices and measurements. Med Prog Tech 1991; 17:249–57.

[6] Munk OL and Bass L. A method to estimate dispersion in sampling catheters and to calculate dispersion-free blood time-activity curves. Med. Phys 2008; 35:3471-81.

[7] Senda M, Nishizawa S, Yonekura Y, Mukai T, Saji H, Konishi J, and Torizuka K. Measurement of arterial time-activity curve by monitoring continuously drawn arterial blood with an external detector: errors and corrections. Ann Nucl Med 1988; 2:7–12.

[8] Boellaard R, Lingen A, Balen SC, Hoving BG, and Lammertsma AA. Characteristics of a new fully programmable blood sampling device for monitoring blood radioactivity during PET. Eur J Nucl Med 2001; 28:81–9.

[9] Convert L, Brassard GM, Cadorette J, Archambault M, Bentourkia M, and Lecomte R. A new tool for molecular imaging: the microvolumetric {beta} blood counter. J Nucl Med 2007;48:1197-2006.

[10] Dhawan V, Jarden JO, Strother S, and Rottenberg DA. Effect of blood curve smearing on the accuracy of parameter estimates obtained for 82Rb/PET studies of blood-brain barrier permeability. Phys Med Biol 2008; 33:61–74.

[11] Takikawa S, Dhawan V, Spetsieris P, *et al*. Noninvasive quantitative fluorodeoxyglucose PET studies with an estimated input function derived from a population-based arterial blood curve. Radiology 1993; 188:131-36.

[12] Eberl S, Anayat AR, Fulton RR, Hooper PK, and Fulham MJ. Evaluation of two population-based input functions for quantitative neurological FDG PET studies. Eur J Nucl Med 1997;24:299–304.

[13] Wakita K, Imahori Y, Ido T, *et al*. Simplification for measuring input function of FDG PET: investigation of 1-point blood sampling method. J Nucl Med 2000; 41:1484–90.

[14] Gambhir S, Schwaiger M, Huang SC, Krivokapich J, Schelbert H, Nienaber C, and Phelps ME. Simple noninvasive quantification method for measuring myocardial glucose utilization in humans employing positron emission tomography and fluorine-18 deoxyglucose. J Nucl Med 1989; 30:359–66.

[15] Iida H**,** Rhodes **G**, Silva R, Araujo L, Bloomfield P, Lammertsma AA, and Jones T. Use of the left ventricular time-activity curve as a noninvasive input function in dynamic oxygen-15-water positron emission tomography. J Nucl Med 1992; 33:1669–77.

[16] Ferl GZ, Zhang X, Wu HM, and Huang SC. Estimation of the ^{18}F-FDG input function in mice by use of dynamic small-animal PET minimal blood sample data. J Nucl Med 2001; 42:1622-29.

[17] Kim J, Herrero P, Sharp T *et al*. Minimally invasive method of determining blood input function from PET images in Rodents. J Nucl Med 2006; 47:330-36.

[18] Buvat I, Benali H, Rouin F, Bazin JP, and Di-Paola R. Target apex-seeking in factor analysis of medical image Sequences," Phys Med Biol 1993;38:123–38.

[19] Wu HM, Hoh CK, Choi Y *et al*. Factor analysis for extraction of blood time-activity curves in dynamic FDG-PET studies. 1995; 36:1714-22.

[20] Sitek EV, Bella D, and Gullberg GT, "Factor analysis with *a priori* knowledge - application in dynamic cardiac SPECT. Phys Med Biol 2000; 45:2619–38.

[21] Hsiao-Ming W, Hoh KC, Choi RY, Schelbert H, Randall A, Phelps ME, and Huang SC. Factor Analysis for Extraction of Blood Time-Activity Curves in Dynamic FDG-PET Studies. J Nucl Med 1995; 36:1714–22.

[22] Naganawa M, Matani A, Kimura Y. Extraction of vessel-related information from PET images without continuous blood sampling using modified independent component analysis, in: Proceeding of the 23rd Annual International Conference of the IEEE Engineering in Medicine and biology Society, Istanbul, 2001, pp:2744 – 47.

[23] Naganawa M, Kimmura Y, Oda K, Ishiwata K, and Matani A. Extraction of a plasma time-activity curve from brain PET images based on independent component analysis. IEEE Trans Biomed Eng 2005; 52:201-10.

[24] Naganawa M, Kimmura Y, Ischii K, Oda K, and Ishiwata K. Temporal and special blood information estimation using Bayesian ICA in dynamic cerebral positron emission tomography. IEEE Digital Sign Processing 2007; 17:973-93.

[25] Naganawa M, Tsukada H, Ohba H, Ishiwata K, Seki C, Shidahara M, and Kimura Y. Omission of serial arterial blood sampling for quantitative analysis of monkey PET data using independent component analysis-based method. IEEE Nucl Sci Symp Conference Record, 2007

[26] Su KH, Lee JS, Li JH, Yang YW, Liu RS and Chen J C. Partial volume correction of the microPET blood input function using ensemble learning independent component analysis. Phys Med Biol 2009; 54:1823–46.

[27] Mendez MM, Juslin A, Nesterov VS, Kalliokoski K, Knuuti J, and Ruotsalaine U. ICA Based Automatic Segmentation of Dynamic H215O Cardiac PET Images. IEEE Trans on Inform tech in Biomed 2010; 14:795–802.

[28] Van der Weerdt AP, Klein LJ, Boellaard R, Visser CA, Visser FC, and Lammertsma AA. Image-derived input functions for determination of MRGlu in cardiac 18F-FDG PET scans. J Nucl Med 2001; 42:1622–29.

[29] Fang Y and Muzic R. Spillover and partial-volume correction for image-derived input functions for small-animal 18F-FDG PET Studies. J Nucl Med 2008; 49:606–14.

[30] Wong KP, Feng D, Meikle SR, and Fulham MJ. Simultaneous estimation of physiological parameters and the input function - in vivo PET data. IEEE Trans Inform on Tech in Biomed 2001;5:67-76.

[31] Selivanov V, Lapointe D, Bentourkia M, and Lecomte R. Cross-validation stopping rule for ML-EM reconstruction of dynamic PET series: Effect on image quality and quantitative accuracy. IEEE Trans Nucl Sci 2001; 48:883–9.

[32] Phelps ME, Huang SC, Hoffman EJ, Selin C, Sokoloff L, and Kuhl DE. Tomographic measurement of local cerebral glucose metabolic rate in humans with (F-18)2-fluoro-2-deoxy-d-glucose: validation of method. Annals of neurology 1979; 6:371–88.

[33] Shi X and Manduchi R. A Study on Bayes Feature Fusion for Image Classification. Conference on Comp Vision and Patt Recog Workshop, 2003.

[34] Gorsevski PV, Gessler PE, and Jankowski P. Integrating a fuzzy k-means classification and a Bayesian approach for spatial prediction of landslide hazard. J Geograph Syst 2003; 5:223–51.

[35] Kass RE and Raftery AE. Bayes Factors. J Am Statist Assoc 1995; 90:773-795.

[36] Raymond F, Muzic J, and Cornelius S. COMKAT: Compartment Model Kinetic Analysis Tool. J Nucl. Med 2001; 42:636–45.

[37] Wu HM, Guodong S, Lee C, Prins M, Ladno W, Lin H, Yu A, Phelps ME, and Huang SC. Mouse plasma and whole blood difference in 2-[^{18}F]fluoro-2-deoxy-D-glucose (^{18}F-FDG) concentration: implication for quantitative mouse 18F-FDG PET studies. J Nucl Med 2007; 48:837–45.

[38] Gregory ZF, Xiaoli Z, Hsiao-Ming W, and Sung-Cheng H. Estimation of the 18F-FDG Input Function in Mice by Use of Dynamic Small-Animal PET and Minimal Blood Sample Data. J Nucl Med 2007; 48:2037–45.